25

Optimal Selection of Drive Components for Doubly-Fed Induction Generator Based Wind Turbines

Dr. Davide Aguglia[1,2], Prof. Philippe Viarouge[1],
Prof. René Wamkeue[3] and Prof Jérôme Cros[1]
[1]*LEEPCI Laboratory, Laval University, G1K 7P4 Quebec (QC)*
[2]*CERN – European Organization for Nuclear Research,*
Electric power converter Group, CH- 1211 Geneva 23
[3]*UQAT, Abitibi-Témiscamingue Quebec University,*
J9X 5E4 Quebec (QC)
[1,3]*Canada*
[2]*Switzerland*

1. Introduction

This chapter presents recent advancements and global design methods, as well as new results, regarding the electromechanical drive of wind turbines equipped with Doubly-Fed Induction Generators (DFIG). Currently DFIG is the most popular topology used by the large wind turbine manufacturers, because a wide variable speed range with a reduced static converter size can be obtained with a suitable control of the real and reactive power flows (Pena et al., 1996). The variable speed operation of wind generation systems presents several advantages that have been well established in the literature (Zigner et al., 1997) and improves the annualized wind energy yield. However the design process of such an electromechanical system needs suitable compromises between the performances of the wind turbine on the whole speed range and the respective characteristics of the induction machine, the gearbox and the static converters. The optimal solution in terms of performance and cost must be derived from a global design approach. For a given turbine, a given DFIG and a given annual wind distribution, a suitable compromise must be found between the gearbox ratio and the sizing of the power converters to maximize the annual energy yield. The choice of the gearbox ratio for variable speed DFIG is not detailed in the literature. This chapter presents a methodology that can be used for the optimal determination of at least these two important variables of the design process in terms of annual energy yield and initial cost. To demonstrate the advantages of the use of a global approach to define the best compromises in terms of relative size between the drive components and control laws is one of this chapter's goals.
Figure 1 presents the structure of the topology under study, which is using a four quadrants variable frequency static converter.
The purpose of this global approach is to determine the optimal dimensioning, or sizing, compromises to be adopted in order to optimize the overall performances of the

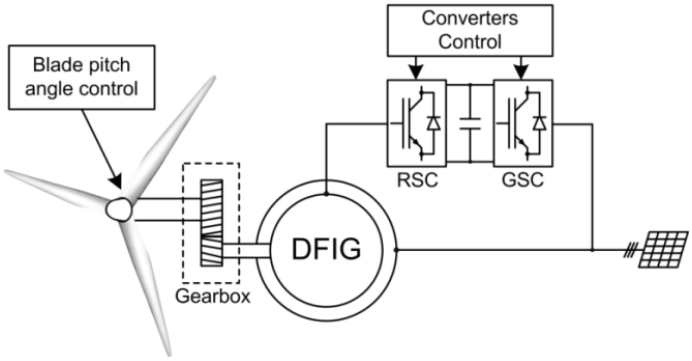

Fig. 1. Structure of the DFIG based wind turbine under study.

electromechanical drive. For instance one has to define the gearbox ratio, the power converter rating and the steady-state control laws which are maximizing the wind turbine annual production at minimal cost and minimal mass installed into the nacelle (Aguglia et al., 2007a). A global analysis is needed to achieve this objective. In the industry, each drive component is offered by a different supplier, and the final assembly doesn't necessarily represent a globally optimized solution in terms of sizing or cost. Except recent publications from the authors of this chapter, such an approach is not presented in the literature. The annual production of a wind turbine is one of its most important global performances. The higher the energy production, the higher the investment returns. To determine the annual production of a wind turbine one has to adopt a global analysis, by obtaining all the necessary models which allow the prediction of the losses of all sub-components of the drive. Furthermore, because the annual production depends on the wind statistics of a given site, the models used for its computation should be flexible enough to allow the computation of losses for any operation point of the plant, characterized by the generator torque, the rotating speed and the electrical power factor. The chapter will present the method allowing taking into account a statistical and cyclical operation of such a plant (Aguglia et al., 2007b). For each operating point of the plant, the rotor phasor voltage and the current imposed, or controlled, by the Rotor Side Converter (RSC) (refer to Fig. 1) must be imposed by a suitable control law to optimize the performance. To obtain a fast computation of the overall performances of the system on the whole variable speed range, one needs to obtain the RSC control laws for each operating point. A novel analytical method to derive such laws is also presented in the chapter (Aguglia et al., 2008). Once all the performances can be easily determined on the whole variable speed range, it is possible to perform a sizing analysis. For instance, it is possible to determine the annual production versus the dimensional constraints or the total mass installed into the nacelle. This chapter presents guidelines to answer to the following questions:

- How to select the gearbox ratio in order to optimize the annual production?
- What is the influence of the maximal voltage delivered by the RSC on the annual production? (DC-Bus voltage limit imposed by the switches technology).
- What is the influence of the maximal power converter apparent power selection on the variable speed range and the annual production?
- What are the compromises between the annual production and the total mass installed into the nacelle?

2. Models of the wind energy conversion system

2.1 Wind and wind turbine models

The wind site model is based on a *Weibull* probability distribution function of the wind speed (Heier, 2006). Figure 2(a) presents an example of such wind speed distribution for a site with an annual average wind speed of 6 [m/s]. Expression (1) is used to compute the mechanical power delivered by the wind turbine. A typical characteristic of the maximal power against wind speed is presented in Fig. 2(b).

$$P_t = \frac{1}{2} C_p(\lambda, \beta) \rho_{air} \pi r_{turb}^2 v^3 \tag{1}$$

ρ_{air} , r_{turb} and v are the air density, the wind turbine radius and the wind speed respectively. The factor C_p is the power coefficient that depends on the tip speed ratio (2) and the blade pitch angle β.

$$\lambda = \frac{r_{turb} \Omega_{turb}}{v} \tag{2}$$

Fig. 2(d) presents the variations of C_p against the tip speed ratio λ for different values of pitch angle β. An analytical expression for C_p can be found in (Heier, 2006). The C_p factor must be maintained to its maximal value to optimize the output mechanical power of the turbine on the whole wind speed range. For this purpose, the tip speed ratio must be kept constant at its optimal value. According to (2), the rotational speed of the turbine must remain proportional to the wind speed as presented in Fig. 2(c).

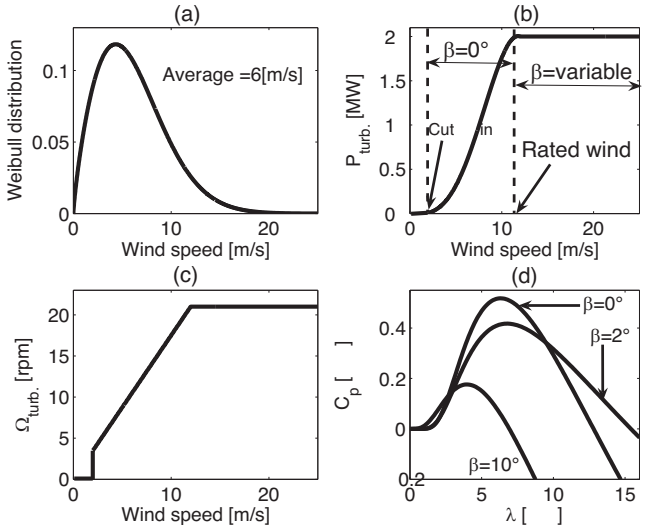

Fig. 2. Wind statistics and wind turbine steady-state characteristics. (*Weibull* distribution (a), Maximal power (b), optimal rotating speed profile (c), and power coefficient C_p (d) against wind speed).

2.2 Gearbox losses and mass models

The gearbox losses can be approximately modeled by constant viscous losses. Since gearboxes for wind turbines equipped with DFIGs are usually composed of three stages, the oil friction losses are higher in the second and third stages because their rotating speed is higher. A viscous loss proportion of 1% of rated power per stage is a reasonable assumption (Cotrell, 2002). The gearbox efficiency and its mechanical losses can be determined by (3).

$$\eta_{gearbox} = \frac{P_{Into\,gearbox} - q \cdot 0.01 \cdot P_{rated\,gearbox}}{P_{Into\,gearbox}}$$
$$P_{gearbox\,losses} = P_{\max gearbox\,losses} \frac{n}{n_{rated}} \tag{3}$$

q is the number of gearbox stages, n is the actual rotor speed (rpm) and n_{rated} is the rated rotor speed (rpm). The gearbox mass is also an important factor of the design of a DFIG drive system. For DFIG wind turbines in the MW range, the gearbox mass can be twice the DFIG mass. According to the data available in (Flender, 2006), the gearbox mass depends on the torque on the low speed shaft and on the number of stages. For example, the mass of a three-stage gearbox of 2 [*MW*] with a low rotating speed of 19 [*rpm*] and a torque of 1.06 [*MNm*], is equal to 8.5 Tons. Its speed ratio G_r can be selected in a range between $45<G_r<125$. For lower speed ratios, the gearbox has two stages only. In this case, the mass is 7.8 Tons and the ratio range is $25<G_r<40$. For single stage gearboxes in the *MW* power range, the speed ratio is between $3<G_r<8$. The mass model of single stage gearboxes is described by the following equation (Li et al., 2009):

$$M_{Gear} = \frac{3.2 T_n F_s F_m}{1000} \tag{4}$$

Where T_n is the nominal torque on the high speed output, F_s the service factor (F_s=1.25 is used here) and F_m is the mass factor defined as in (5).

$$F_m = \frac{1}{Z} + \frac{1}{Z r_w} + r_w + r_w^2 + 0.4 \frac{1 + r_w}{Z} \left(G_r - 1\right)^2 \tag{5}$$

Were Z is the number of satellites ($Z=6$ is used here) and r_w is a factor defined as $r_w=(G_r/2)-1$.

2.3 Doubly-Fed induction generator model

The DFIG steady-state model is based on the classical wounded rotor induction machines equivalent circuit depicted in Fig. 3. From this circuit the overall performances of the DFIG can be derived, if both stator and rotor power supplies are defined. Compared to the classical induction machine, the DFIGs electromagnetic torque derivation is slightly different and is presented in section 3.1.

2.4 Static power converter losses model

The total losses of the back-to-back PWM VSI converter can be derived from (6). This loss model is based on the parameters of conventional 1700*V* IGBT modules, with a switching frequency of 5 [*kHz*], and a third harmonic injection process (Peterson, 2005).

$$
\begin{aligned}
P_{losses,conv} &= P_{losses,RSC} + P_{losses,GSC} \\
&= 3\left(3.88\frac{\sqrt{2}\cdot 2}{\pi} I_{RSC} + \frac{1.76}{2I_{RSC,\max}} {I_{RSC}}^2 \right) \\
&\quad + 3\left(3.88\frac{\sqrt{2}\cdot 2}{\pi} I_{GSC} + \frac{1.76}{2I_{GSC,\max}} {I_{GSC}}^2 \right)
\end{aligned} \tag{6}
$$

I_{RSC} and I_{GSC} are the respective *rms* values of the line currents of the rotor and grid side converters.

3. Wind power plant control

3.1 DFIG torque control

The analytical determination of the control laws presented in this paper doesn't take into account the mechanical and magnetic losses of the drive. The steady-state equivalent circuit of the induction generator is presented in Fig. 3.

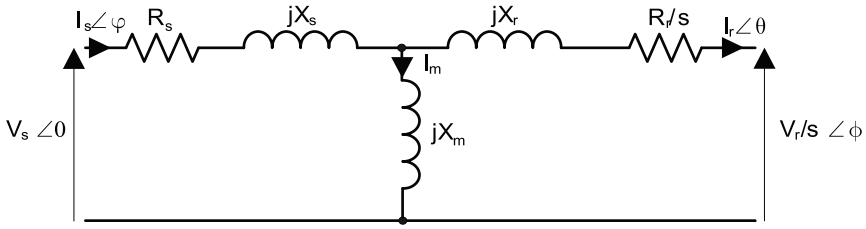

Fig. 3. DFIG Equivalent circuit.

The generator air gap power P_{ag} is:

$$P_{ag} = 3\frac{R_r}{s} I_r^2 + 3\frac{V_r}{s} I_r \cos(\phi - \theta) \tag{7}$$

All the phase angles are referred to the stator voltage V_s, except for the rotor phase angle $\psi = \phi - \theta$ that is the angle between the rotor current and the rotor voltage. Therefore, the electromagnetic torque T_e can be written as:

$$
\begin{aligned}
T_e &= \frac{3p}{\omega_s}\left[\frac{R_r}{s} I_r^2 + \frac{V_r}{s} I_r \cos(\psi) \right] \\
&= \frac{p}{\omega_s s}\left[3R_r I_r^2 + P_r \right]
\end{aligned} \tag{8}
$$

Equation (8) shows the influence of rotor voltage V_r and phase angle ψ on the electromagnetic torque. From the same equation, one can notice that the active power flow P_r in the RSC controls the electromagnetic torque of the DFIG. Because there are two control variables, the same torque T_e value (or power P_r) can be obtained with different combinations of V_r-ψ pairs but with different performances in terms of efficiency and power factor.

3.2 Novel analytical determination of converter control laws

The rotor side power converter control strategy has a direct influence on the DFIG performance. Several approaches have been proposed in the literature to determine specific rotor converter control laws that minimize some objective function like the total drive losses for example. Non-linear constrained optimization techniques have been proposed for this purpose (Çadirici et al., 1992) (Smith et al., 2005). But these approaches can be problematic if the determination of the control law must be performed for each step of a DFIG global design process that is also based on the use of a non-linear constrained optimization procedure. Two embedded optimization methods in the same CAD environment can lead to convergence problems and drastically increase the total number of iterations (see Fig. 4).

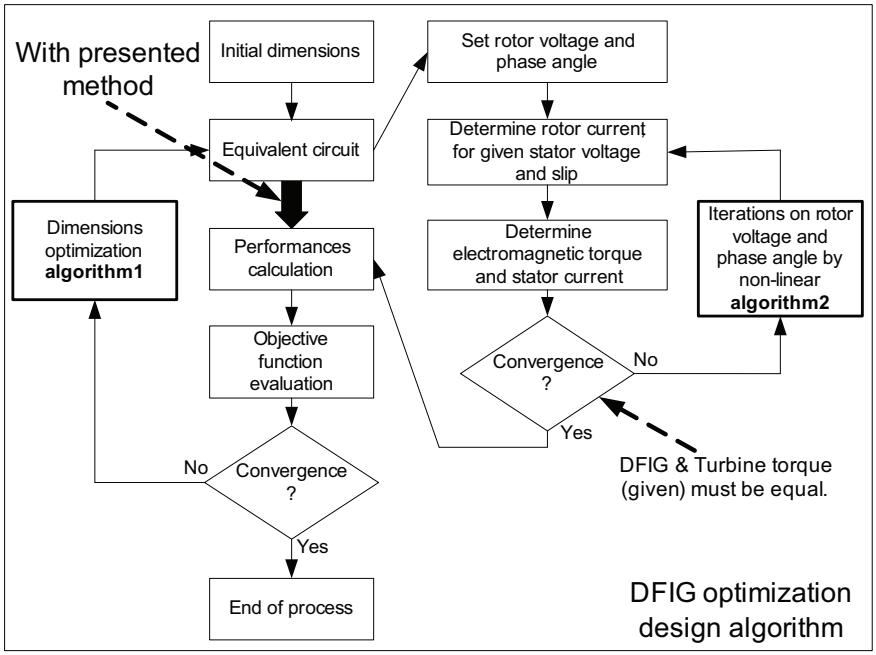

Fig. 4. DFIG global design process with two embedded non linear optimization methods

It is possible to find an analytical solution for the determination of the rotor control laws to avoid the use of the non-linear algorithm 2 in Fig. 4. A single solution for the rotor control variables V_r and ψ exists for each steady-state operation point because the electromagnetic torque and the generator stator power factor are imposed by the wind turbine torque-speed characteristic and the grid specifications.

Fig. 5 illustrates the method that is proposed to derive the analytical formulation of the rotor control laws. For each steady-state operation point, the generator electromagnetic torque T_e is considered to be equal to the output mechanical torque T_t of the turbine since the mechanical losses are neglected. The stator voltage V_s and the stator power factor SPF=$cos\varphi$ (where φ is the phase angle between the fundamental components of the stator current and voltage) are imposed because the grid power factor GPF is fixed by the grid specifications and the grid side converter power factor is equal to unity.

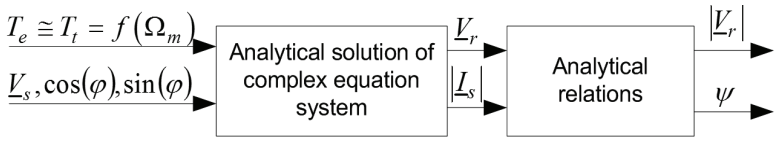

Fig. 5. Diagram of the procedure for the analytical determination of converter control laws.

It is common to operate the rotor side converter to deliver the reactive power absorbed by the DFIG and to keep the grid side converter at unity power factor. This strategy is preferable because the voltage delivered by the rotor side converter is multiplied by a factor 1/s before being applied to the magnetizing inductance of Fig. 3, which is absorbing the main part of the total DFIG reactive power. If the voltage drop across the rotor resistance and leakage inductance are neglected, the total DFIG reactive power can be expressed as in (9).

$$Q_m \cong 3\left(\frac{V_r}{s}\right)^2 \frac{1}{X_m} \cong 3\frac{1}{s} V_r I_r \sin(\psi) \cong \frac{1}{s} Q_{RSC} \tag{9}$$

Since the value of the slip *s* is always less than unity, it is preferable to compensate the DFIG reactive power consumption with the RSC. A system of three analytical equations can be established to derive the three intermediate variables listed on Fig. 5 (*rms* value of the stator current I_s, real and imaginary components of $\underline{V}_r$) from the input parameters T_t, V_s , *cosφ* and *sinφ*. The Thévénin equivalent circuit of the DFIG depicted in Fig. 6 is used for this purpose.

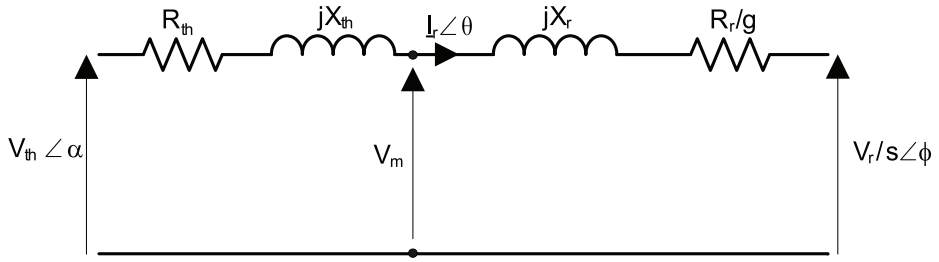

Fig. 6. DFIG Thévénin equivalent circuit.

The parameters R_{th} and X_{th}, and the voltage V_{th} can be derived from the stator voltage V_s, the resistance R_s, the reactances X_s and X_m, by applying the Thévénin transformation on the equivalent circuit of Fig. 3. Several intermediate variables are listed in (10):

$$\begin{aligned} &\underline{V}_s = V_s + j0 \\ &\underline{V}_{th} = V_{thr} + jV_{thi} = V_{th}^{\angle\alpha} \\ &\underline{V}_r = a + jb = V_r^{\angle\phi} \\ &\underline{I}_s = c \cdot \cos(\varphi) + jc \cdot \sin(\varphi) = c \cdot x + jc \cdot y = I_s^{\angle\varphi} \end{aligned} \tag{10}$$

The three unknown variables *a, b* and *c* in (10) can be determined with a set of three equations. The first two equations can be derived by computing the rotor complex current $\underline{I}_r$ in the equivalent circuits of Fig. 3 and Fig. 6. Equation (11) leads to a system of two equations, one for the real part and another for the imaginary part of the rotor current.

$$I_r = I_s - I_m = \frac{V_{thr} + jV_{thi} - \dfrac{a+jb}{s}}{R_{th} + \dfrac{R_r}{s} + j\left(X_{th} + X_r\right)} = c \cdot x + jc \cdot y - \frac{V_s - \left(c \cdot x + jc \cdot y\right)\left(R_s + jX_s\right)}{jX_m} \tag{11}$$

The third equation is derived from the DFIG torque equation that must be equal to the turbine torque under steady-state operation. In (12) the electromagnetic torque is a function of the stator current, the rotor voltage and the DFIG parameters only. The system of equations (11) and (12) can be solved to determine the variables *a*, *b* and *c* and derive the rotor voltage and stator current.

$$T_e = T_t = \frac{3p}{\omega_s}\left(\begin{array}{l} \dfrac{R_r}{s}\left(\left(c \cdot x + \dfrac{c \cdot xX_s + c \cdot yR_s}{X_m}\right)^2 + \left(c \cdot y + \dfrac{V_s - c \cdot xR_s + c \cdot yX_s}{X_m}\right)^2\right) + \\ \dfrac{c \cdot xa + c \cdot yb}{s} + \dfrac{bV_s - c \cdot xR_s b + c \cdot xX_s a + c \cdot yR_s a + c \cdot yX_s b}{X_m s} \end{array}\right) \tag{12}$$

The symbolic analytical solution of such a complex system of equations was performed by use of *Mathematica*®. The complex rotor current $\underline{I}_r$ and the phase angle ψ can be finally derived from equations (13) and (14) obtained with the equivalent circuit of Fig. 3.

$$\underline{I}_r = \frac{-\left(V_s - \underline{I}_s\left(R_s + jX_s\right)\right)}{jX_m} + \underline{I}_s \tag{13}$$

$$\psi = \arctan\left(\frac{\mathrm{Im}\left(\underline{I}_r\right)}{\mathrm{Re}\left(\underline{I}_r\right)}\right) - \arctan\left(\frac{\mathrm{Im}\left(\underline{V}_r\right)}{\mathrm{Re}\left(\underline{V}_r\right)}\right) \tag{14}$$

The efficiency of the DFIG is:

$$\eta = \frac{3\left[V_r I_r \cos\left(\psi\right) - V_s I_s \cos\left(\varphi\right)\right]}{3\left[V_r I_r \cos\left(\psi\right) - V_s I_s \cos\left(\varphi\right) + R_s I_s^2 + R_r I_r^2\right] + P_{mags} + P_{magr}} \tag{15}$$

One can notice that the magnetic losses are included in the efficiency formulation These losses are computed from the DFIG dimensions and magnetic induction levels. The stator magnetic losses P_{mags} are nearly constant because a constant voltage/frequency ratio is imposed by the grid at the stator terminals. The rotor magnetic losses P_{magr} that are not negligible because of large slip operation are also computed.

3.3 Variable speed range limitations

To maximize the energy production of the power plant, the turbine rotating speed must vary with the wind speed in order to maintain the tip speed ratio λ at its optimal value (see eq. (1) and (2)). As visualized in Fig. 2 the turbine rotating speed should vary linearly with the wind starting from very low wind speeds values up to the nominal wind and rotating speeds. One has to verify that the generator is able to guarantee such a variable speed range. A limiting factor is provided by the voltage limitation introduced by the rotor power converter. To understand this phenomena suppose that stator and rotor windings

resistances and leakages inductances are negligible (which is a legitimate hypothesis, especially for large generators). Then, the DFIG equivalent circuit is reduced to impedance represented by the magnetizing inductance only as shown in Fig. 7.

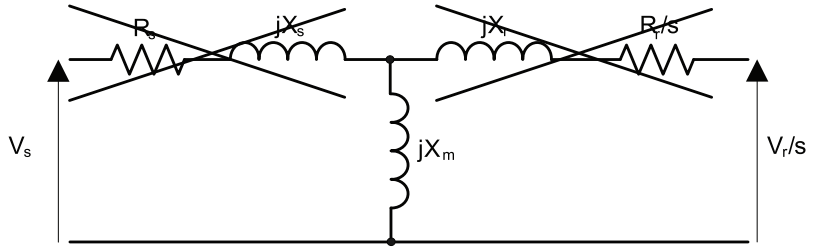

Fig. 7. DFIG equivalent circuit assuming no voltage drop across winding resistances and leakage inductances.

Based on this assumption one is allowed to write the following identity:

$$V_s = \frac{V_r}{s} \tag{16}$$

The voltage V_r is referred to the stator side. If we define *sr* as the stator to rotor windings turns ratio, or the stator to rotor voltages ratio when the DFIG is at standstill (neglecting the windings pitch and distribution factors), we can rewrite (16) as:

$$V_s = \frac{V_r' sr}{s} \tag{17}$$

V_r' represents the voltage at the rotor side converter terminals, which has an amplitude limitation imposed by the switches technology. For instance, the use of $1700V$ IGBT technology limits the power converter DC-Bus voltage to approximately $1000V$ to $1200V$. Therefore, the maximal *rms* phase voltage which can be handled by the rotor side converter is in the order of $1000\text{V}/(\sqrt{2}\sqrt{3}) \cong 400V$. Considering eq. (17) one notices that since the stator voltage V_s is fixed and imposed by the grid, and since the stator to rotor turns ratio *sr* cannot vary, when the power converter voltage V_r' has reached its maximal value, the slip *s* is not allowed to vary anymore (respect of eq. (17)). This means that as soon as the maximal rotor voltage is reached, the wind turbine must operate at constant speed even if the wind speed is varying. This situation can appear during low wind speeds operations where the slip *s* and the rotor voltage V_r' are very large (eq. (17)). This equation reveals another important issue; the selection of stator to rotor turns ratio *sr*. Usually the maximal rotor voltage at the converter terminals is equal to the stator voltage V_s. In steady-state operation of the wind turbine the rotor voltage is always kept below its maximal value in order to guarantee a voltage margin for torque-speed correction (e.g. wind gusts). It is usual to keep a safety rotor voltage margin of 25% (Petersson, 2005), which means that the maximal rotor side converter voltage during steady state operation is about $300V$. For instance, supposing that the maximal slip is $s=0.3$, one can approximately derive the stator to rotor turns ratio as shown in (17).

$$sr = \frac{sV_s}{V_r'} = \frac{0.3 \cdot 400V}{300V} = 0.4\ [-] \tag{18}$$

Here it is easy to understand that due to the voltage limitation, and due to the objective of maximizing the variable speed range, the selection of the power converter maximal voltage (rating), the placement of the synchronous speed with respect to the wind speed, i.e. the maximal slip s which can be adjusted with the selection of the gearbox ratio, and the selection of the stator to rotor turns ratio sr, in not a trivial process and needs a global optimization approach.

3.4 2.5 MW wind turbine performances illustration by numerical simulation

The parameters of a typical 2.5 MW wind generator using a DFIG system have been used to illustrate the proposed analytical method to derive the control law. All needed parameters are presented in Table 1.

Rated power	2.5	MW
Rated voltage	690	V
Base frequency	50	Hz
Stator resistance	0.045	p.u.
Rotor resistance	0.028	p.u.
Stator leakage inductance	0.077	p.u.
Rotor leakage inductance	0.15	p.u.
Mutual inductance	3.3	p.u.
Number of poles-pairs	3	-
Rotor diameter	80	m
Rated wind speed	15	m/s
Turbine speed range	10.9-19.1	rpm
Gearbox ratio	1:68.1	-

Table 1. 2.5 MW DFIG and wind turbine parameters used for simulations.

The mechanical power collected by a wind turbine can be derived from the kinetic energy of the air flow facing the swept area of the blades as expressed in (1). Figure 8 shows an example of the C_p characteristic as a function of the tip speed ratio, for three different blade pitch angles.

The maximum power characteristic of a real 2.5 MW wind turbine (Nordex, 2007) is presented in Fig. 9(a). The variation of the power coefficient of this turbine versus wind speed is reported in Fig. 9(b) (Nordex, 2007).

One can identify four different wind speed regions of operation on Fig. 9(a). Region 2 coincides to a nearly constant and maximum power coefficient C_p where the blade pitch angle β and the tip speed ratio λ are constant and set to their optimal value. In this region, the output power of the turbine is proportional to the third power of the wind speed (1). At a wind speed of approximately 11 m/s, the maximum rotating speed of the turbine is reached and must be limited to respect the mechanical and aerodynamic constraints. In region 3, the limitation of the rotating speed is provided by a suitable control of the DFIG torque, and the blade pitch angle is controlled in order to track a maximum power coefficient C_p. However, the tip speed ratio λ and the power coefficient C_p are decreasing as

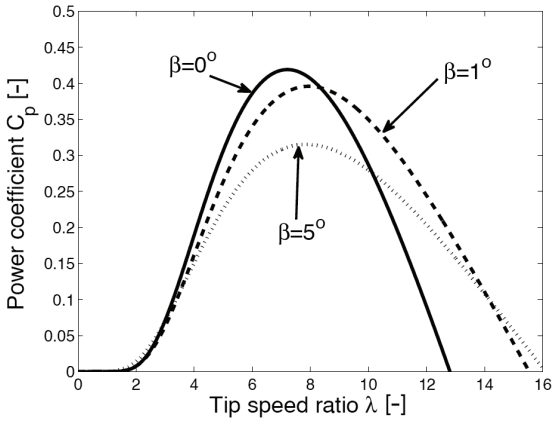

Fig. 8. Typical C_p factor characteristic for MW range wind turbines.

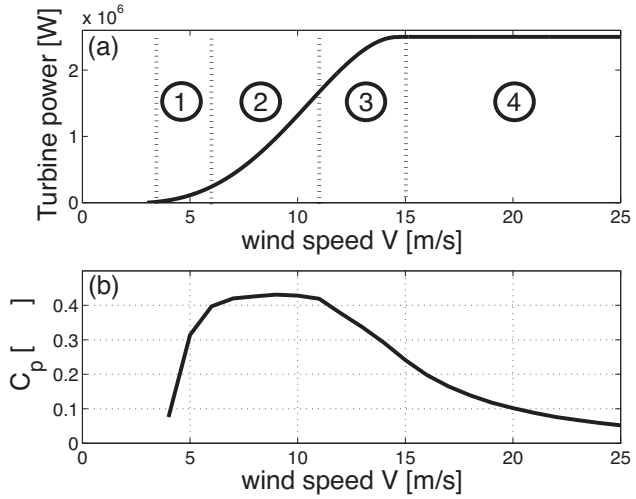

Fig. 9. 2.5 MW Wind turbine power characteristics (Nordex, 2007).

the wind speed increases. The turbine output power is still increasing with the wind speed but with a smaller rate of change *dPt/dV*. When the rated power is reached at *v=15 m/s*, one enters the region 4 where the blade pitch angle β only is controlled in order to limit the turbine output to its rated maximal value. In region 1 the rotating speed is limited to a minimal value that depends on the maximal rotor voltage that can be produced (Analysis of section 3.3). The wind speed is varying while the rotating speed is fixed, leading to a decrease of the C_p factor (see Fig. 9(b) in region 1). By using the data of Table 1, it is possible to determine the rotating speed versus wind speed control characteristic of the DFIG (Fig. 10(a)) and the turbine output power versus rotating speed characteristic (Fig. 10(b)) which corresponds to the maximum power characteristic of the 2.5 MW wind turbine of Fig. 9(a).

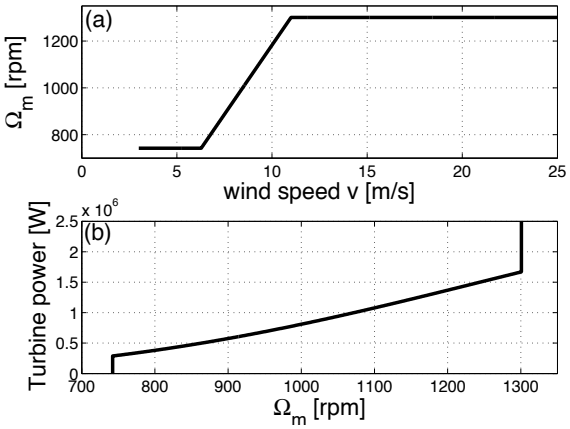

Fig. 10. DFIG rotation speed versus wind speed and turbine power versus rotation speed characteristics.

The DFIG torque characteristic on the whole speed range can be easily derived from the characteristics of Fig. 10 (T=P/Ω).

In this case study, the stator power factor of the generator is set to unity on the whole operation range and the grid side converter (GSC) is operated at unity power factor as well. This leads to a unity power factor operation of the whole system, seen by the grid. With such a strategy, the rotor side converter must deliver the reactive power consumption of the generator only. The steady-state control laws of the rotor side converter, presented in Fig. 11, have been determined by the proposed analytical method. These laws are represented by the characteristics of the two control variables $V_r(\Omega_m)$ and $\Psi(\Omega_m)$. Figure 12 to 15 illustrate the steady-state performances of the whole system on the whole operation range: generator and converter apparent powers, DFIG active power flow, DFIG currents (referred to stator) and DFIG efficiency.

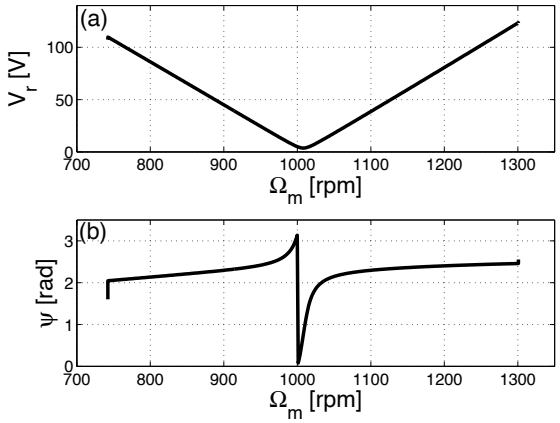

Fig. 11. Rotor voltage and phase angle control law for GPF=1.

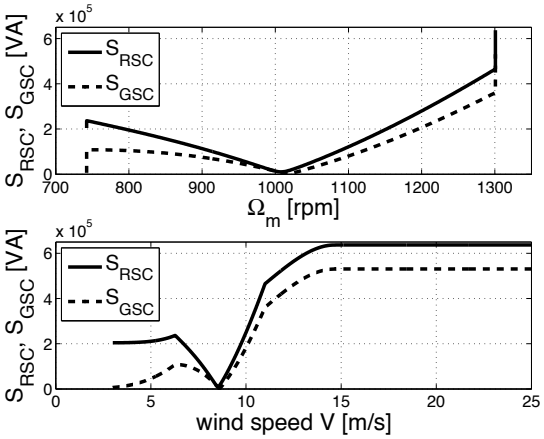

Fig. 12. RSC and GSC apparent power for GPF=1.

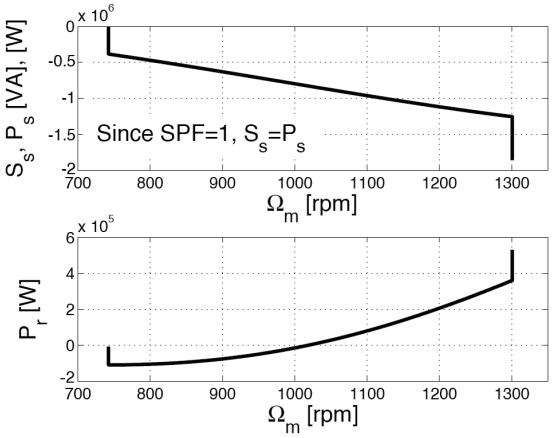

Fig. 13. DFIG powers flows for GPF=1.

The maximal apparent power of the RSC is higher than the maximal apparent power of the GSC since the reactive current is supplied by the RSC. The apparent and active powers of the DFIG stator are identical since the stator power factor is set to unity. One can notice on Fig. 13 that the rotor real power flow P_r is reversed at the synchronous operation speed (1000 [rpm]). The rotor current in Fig. 14 is relatively high in low wind speed regions since the reactive current must always be supplied. In this region, the power extracted from the wind is very low and the rotor copper losses are high; the DFIG efficiency of Fig. 15 is then drastically decreased.

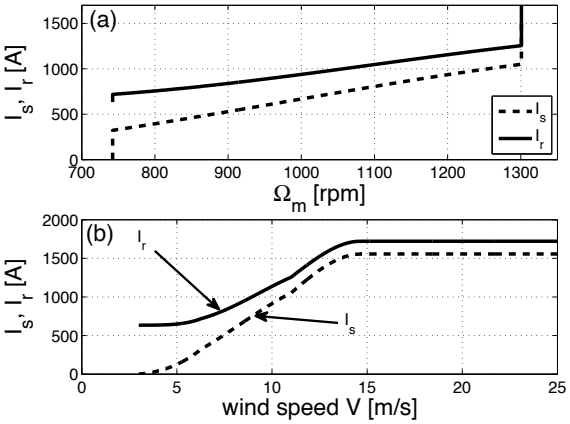

Fig. 14. DFIG stator & rotor RMS currents for GPF=1.

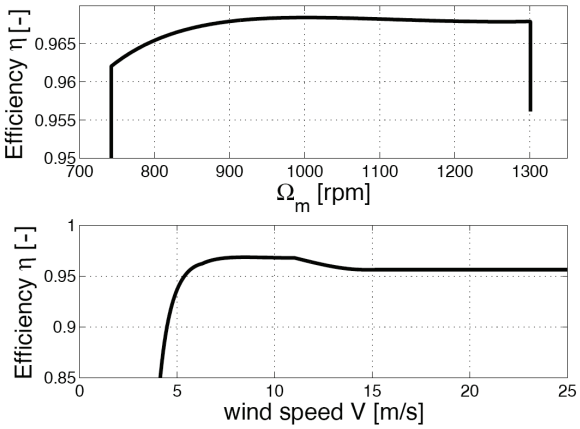

Fig. 15. DFIG Efficiency for GPF=1.

4. Annual energy production

An optimal design must take into account the annual energy production of the plant. It depends on the annual wind distribution of the plant site, on the wind turbine characteristics, on the DFIG, gearbox and power converter losses, and on the control strategy. One computes, for each wind speed, the number of hours of operation and the amount of power extracted by the turbine from the wind flow. The annual mechanical energy production of the turbine can be derived from eq. (19)(Grauers, 1996). $P_t(v)$ is the output power of the turbine and $p(v)$ is the wind probability distribution while the constant 8760 is the number of hours per year.

$$E_{an,turbine} = 8760 \int_{cut-in}^{cut-out} P_t(v)\,p(v)\,dv \tag{19}$$

For a given wind turbine, the annual electrical energy production of the plant is determined by introducing the whole system efficiency. The total losses of the drive system (gearbox, DFIG and power converter) can be computed from the models presented in section 2, for each operation point that corresponds to each wind speed value. One can derive the total efficiency of the drive $\eta_{tot}(v)$ for each wind speed value. The expression for the annual energy yield is expressed in (21).

$$E_{an,grid} = 8760 \int_{cut-in}^{cut-out} P_t(v) p(v) \eta_{total}(v) dv \tag{21}$$

From equation (21) one can notice that the DFIG dimensions, the selected gearbox ratio, the power converter technology or the selection of the stator to rotor turns ratio highly influence the annual energy production. This means that the annual production performance is a suitable performance to be maximized, since it is dependent on all the choices of the drive components.

5. Optimal selection of drive components

5.1 Gearbox ratio selection

The annual energy yield varies with the gearbox ratio since the efficiency of the total wind generation system depends on the exact location of the DFIG synchronous speed operation on the effective wind speed range of the site. The super-synchronous and sub-synchronous speed ranges are changing with the gearbox ratio. This concept is illustrated in Fig. 16 for a given wind turbine and a given DFIG with two different values of the gearbox ratio *Gr1* and *Gr2* (*Gr1*<*Gr2*). The two DFIG rotating speed characteristics are presented on Fig. 16. Since the synchronous speed Ω_s of the DFIG is imposed by the grid frequency and the DFIG magnetic poles number, different sub-synchronous and super-synchronous speed ranges are obtained with different gearbox ratios. The wind speed which coincides to the synchronous speed of the DFIG is changed. If the *Weibull* distribution, describing the wind speeds probability, is taken into account (on top of Fig. 16), one notices that for different gearbox ratios the probability of sub-synchronous or super–synchronous operation is different. The choice of the gearbox ratio is directly related to the annual energy production because the total efficiency of the generation system is different for every rotating speed (e.g. sub-synchronous region efficiency different from super-synchronous region efficiency). Furthermore, the power converter voltage rating is a function of the maximum slip operation (eq. (17)). The choice of the gearbox ratio has direct influence on both the annual energy production and the power converter rating.

A very important aspect to be considered is the gearbox mass, which depends on its speed ratio. As presented in section 2.2, the gearbox mass tends to increase with the gearbox ratio. This has to be considered during the gearbox ratio selection, since it is technically and economically interesting to minimize the mass installed into the nacelle of the wind turbine.

5.2 Power converter apparent power selection

One has to bear in mind that the most important advantage of a DFIG based wind turbine is the low initial cost given by a power converter rated at a fraction of the nominal power only. Therefore, during the design of the DFIG drive, a special attention must be paid to the cost minimization of the power converter in order to maintain the advantage of such topology.

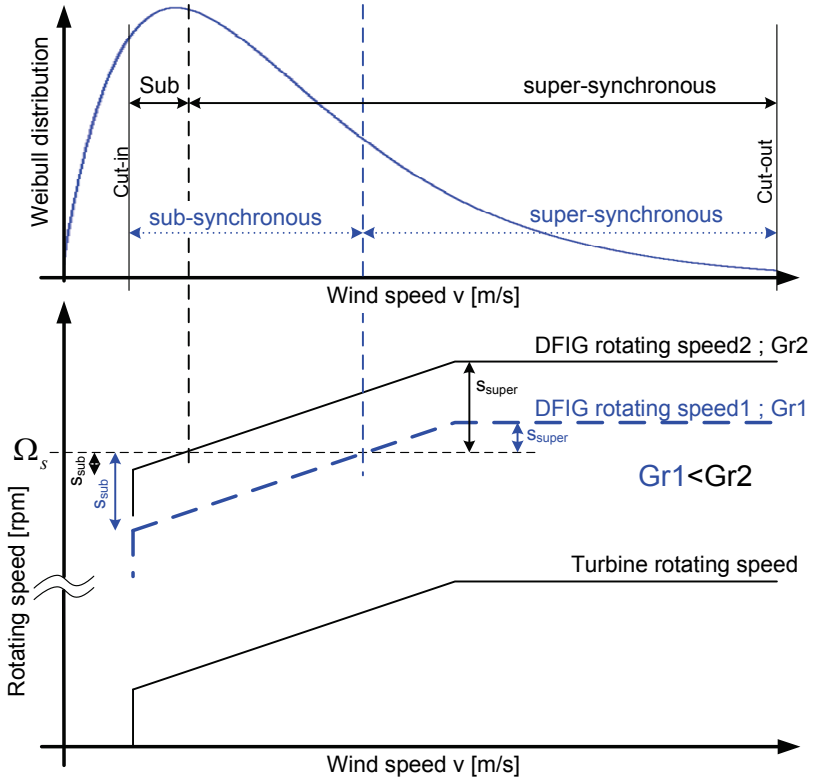

Fig. 16. Effects of the gearbox ratio selection on sub and super-synchronous probabilities of operation.

There are several ways of selecting the power converter rating. To derive the power converter rating one has to define its maximal voltage and its maximal current. The maximal voltage is directly related to the switches technology choice. The maximal current flowing through the power converters is directly related to the maximal active and reactive power flows, which are strongly dependent on the maximal DFIG slip excursion (which in turn is related to the selection of the gearbox ratio). The problematic is that the selection of the gearbox ratio influence the selection of the power converter rating, furthermore all these choices affect the annual production. Because of such complexity it is useful to proceed with an illustration of the influences of every choice on the performances of the wind turbine, this is what is presented in the next section 5.3.

5.3 Illustration of optimal DFIG drive components selection

The selection of the optimal DFIG drive components is an interactive search for optimal compromises between initial cost, mass and energy production. There is no unique and global optimal solution for every specification since all choices have consequences in both technical and economic aspects. As in all engineering domains, technical-economical compromises must be found. The models presented in this chapter can easily be integrated in a non-linear

optimization environment which can be used to determine the optimal selection of the gearbox ratio, the power converter rating and global mass, to optimize an objective function composed by economical and technical performances. However, for the sake of illustration and understanding, this section presents the sensitivity of some global wind turbine performances versus the selection variables. This illustration is based on the wind turbine characterized by the parameters presented in Table 1. Considering a wind site characterized by an average wind speed of μ_v=8m/s and a *Weibull* shape factor k_w=1.8 (Heier, 2006), the annual energy production versus the gearbox ratio selection is presented in Figure 17.

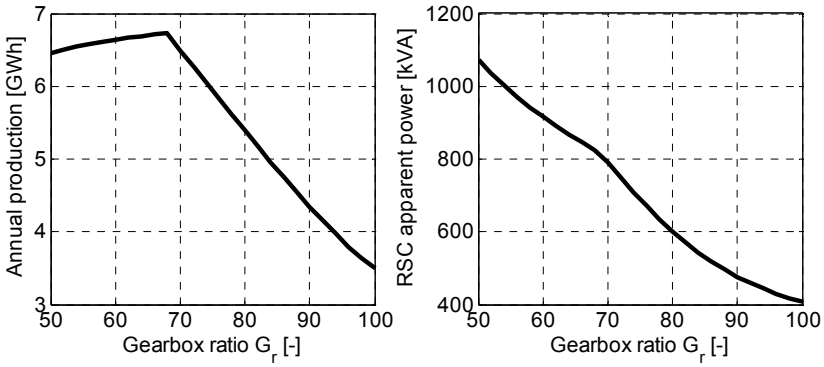

Fig. 17. Annual production and11 rotor side converter maximal apparent (dimensioning) power versus gearbox ratio – 2.5MW wind turbine & average wind speed site of 8 m/s.

The optimal gearbox ratio that is maximizing the annual production is G_r=68.1 [-]. The performances of this configuration are illustrated on figures 8 to 15. However, looking at the power converter (RSC) maximal apparent power (dimensioning power) on the right side of Figure 17, one notices that the higher G_r, the lower the power converter rating. For gearbox ratios higher than G_r=68.1 [-] both the annual production and the power converter rating are drastically decreasing. The considered voltage for the calculation of the RSC apparent power was kept fixed to 690V (line), since the IGBT technology was fixed (1700V IGBTs). To understand the behavior depicted in Figure 17, the visualization of some wind turbine performances versus the wind speed for different gearbox ratios is necessary. This analysis is presented in Figure 18, where turbine power, rotor voltage (rotor side), turbine power coefficient and turbine rotating speed are plotted versus the wind speed for three different gearbox ratios G_r=50, G_r=68.1 and G_r=90.

Solution with G_r=68.1: One can notice that the annual energy is maximized (Fig. 17). From Fig. 18 (b) one notice that the lowest voltage is reached when the DFIG is operating at synchronous speed. An increase of the DFIG slip *s* is associated to a linear increase of the rotor voltage, as showed by the simplified equation (16). The rotor voltage V_r' can increase until it reaches the maximal steady state value (a margin of 25% is kept). Once this limit is reached, either in super-synchronous or in sub-synchronous regions, the DFIG slip *s* is not allowed to vary anymore (eq. (16)) even though the wind speed is changing. Due to mechanical coupling the DFIG speed limitations can be seen on the turbine speed Ω_{turb} of Fig. 18 (d) (10.9 *rpm* and 19.1 *rpm*). This limitation produces regions where the turbine rotating speed is not changing with the wind speed, therefore, recalling eq. (1) and (2) and Fig. 2 (d), such regions present a degradation of the turbine power coefficient C_p (Fig. 18 (c))

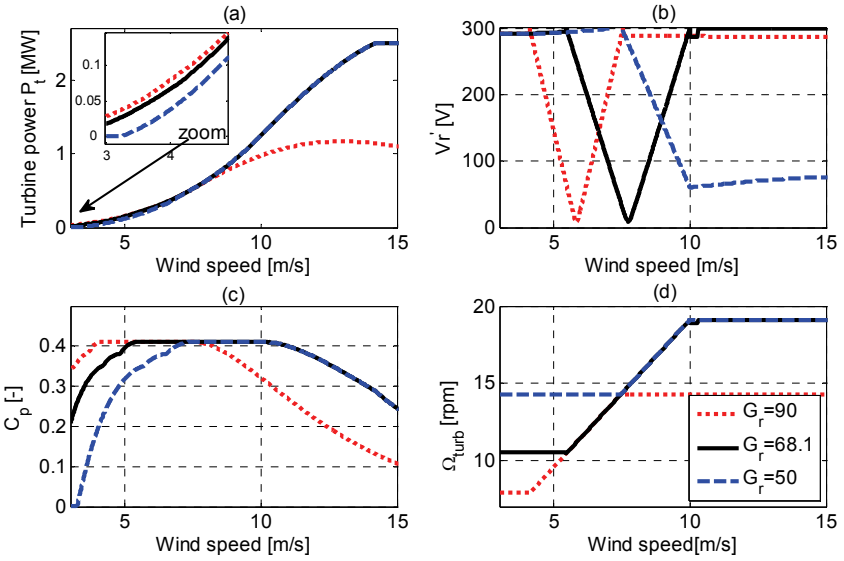

Fig. 18. Turbine power P_t, rotor voltage V_r'(rotor side), turbine power coefficient C_p and turbine rotating speed Ω_{turb} versus wind speed for three different gearbox ratios.

and of the turbine power P_t (zoom of Fig. 18 (a)). The turbine power degradation in the super-sychronous region, starting at a wind speed of 10 *m/s* is noticeable by the fact that Pt is not increasing with the third power of the wind speed anymore, as described by eq. (1). This is the symptom of a decrease of the power coefficient C_p.

Solution with G_r=90: In this case the gearbox ratio is higher, and the DFIG synchronous speed coincides with a lower wind speed (6 *m/s*), as depicted in Fig. 18 (b). As the wind speed increases beyond 6 m/s, the rotor voltage increases with the same rate of change as in the solution with G_r=68.1, since the stator to rotor turns ratio *sr* has not changed (17). Therefore the rotor voltage limit is reached prematurely (7.5 *m/s*) drastically reducing the maximal DFIG and turbine rotating speed (14 *rpm*) as depicted in Fig 18 (d). Consequently the power coefficient C_p experiences a serious degradation (Fig. 18 (c)), causing a dramatic reduction of the wind turbine power P_t in Fig. 18 (a). This is why in Fig. 17 the RSC apparent power is sharply decreasing for high gearbox ratios, since the currents flowing into it decrease with the turbine power decrease.

Solution with G_r=50: Here the gearbox ratio is very low and the DFIG is operating in sub-synchronous only. Therefore the rotor voltage limitation is occurring in the sub-synchronous region in a wide wind speed region (Fig. 18 (b)). This is drastically limiting the minimum turbine rotating speed (fig. 18 (d)), which in turn is degrading the Cp coefficient at low wind speeds. Therefore the turbine power degradation takes place in the lower wind speed region as depicted in the zoom of Fig. 18 (a). This explains why in Fig. 17 the annual energy production is slightly decreasing for low gearbox ratios. It might be surprising that such a slight decrease in the turbine power characteristic, in the low wind speed region, is producing such a loss in the annual production. However one has to consider that at such low wind speeds the *Weibull* distribution can present very high wind probabilities; it is the case in this example.

In this chapter the design of the generator is not discussed, but the simple models previously presented can be used to analyze the importance of the DFIG stator to rotor turns ratio *sr* selection. Figure 19 presents the annual production and the RSC maximal apparent power versus the stator to rotor turns ratio *sr*. In this analysis the gearbox ratio is kept at its optimal value $G_r=68.1$.

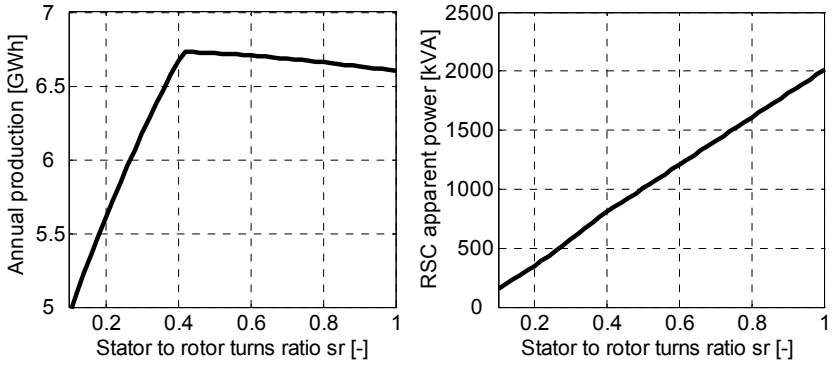

Fig. 19. Annual production and rotor side converter maximal apparent (dimensioning) power versus stator to rotor turns ratio ($G_r=68.1$) – 2.5MW wind turbine & average wind speed site of 8 m/s.

Even in this case one notices an optimal value of *sr* which maximizes the annual production, whereas the RSC maximal apparent power is pseudo-linearly increasing with *sr*. As in the previous analysis of the gearbox ratio selection, the explanation of the curves of Fig. 19 can be given thank to an illustration of some wind turbine performances, versus the wind speed, for several choices of the stator to rotor turns ratio, as proposed in Fig. 20.

Solution with *sr=0.41*: This choice corresponds to the optimal turns ratio that is maximizing the annual energy production as showed in Fig. 19. This case has already been described in the "Solution with $G_r=68.1$" paragraph.

Solution with *sr=0.15*: The value of *sr* is too low in this case. Referring to (17) it is clear that a small variation in the DFIG slip *s*, in the region close to *s=0*, produces a remarkable increase in the rotor voltage. Therefore the rotor voltage limit is reached for very small DFIG slips *s*., as shown in Fig. 20 (b). Thus, the variable speed range is highly reduced (Fig. 20 (d)), producing a degradation of the turbine power coefficient Cp over a wide wind speed region as shown in Fig. 20 (c). Since the rotating speed limitation is occurring in the sub-synchronous and super-synchronous regions, the wind turbine power degradation occurs in the low and high wind speeds regions, explaining the severe decrease of the annual production illustrated in Fig. 19.

Solution with *sr=0.8*: The *sr* value is so low that the rotor voltage increases slowly with the DFIG slip, as shown in Fig. 20 (b). For low wind speeds, where the DFIG is operating in sub-synchronous mode, no rotor voltage limitation is reached. This extends the variable speed range to the low wind speeds region, increasing the turbine power above the values reached in the case with *sr=0.41*, as shown in the zoom of Fig. 20 (a). In the super-synchronous region the rotor voltage never reaches its limitation since the turbine mechanical speed limitation is reached first. This means that this solution maximizes the turbines power to its

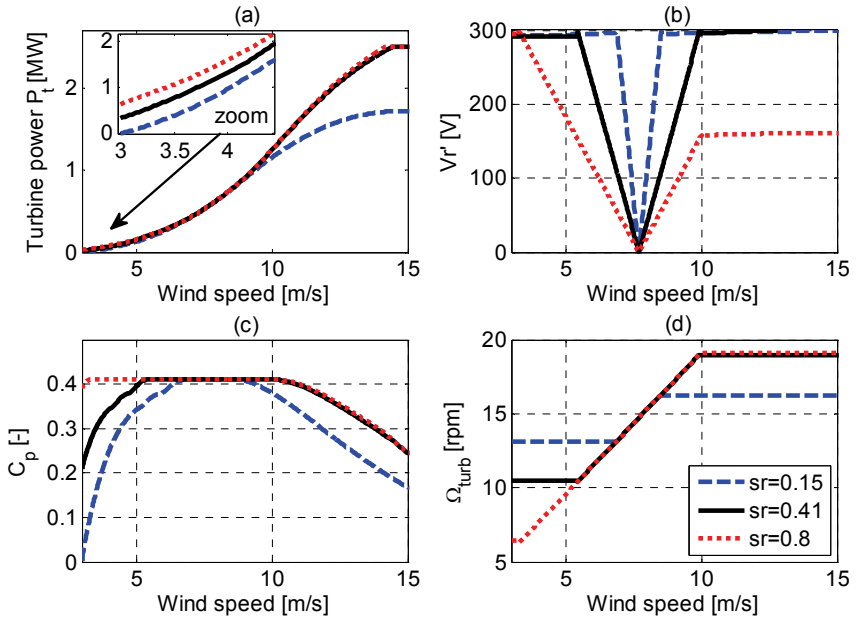

Fig. 20. Turbine power P_t, rotor voltage V_r'(rotor side), turbine power coefficient C_p and turbine rotating speed Ω_{turb} versus wind speed for three different stator to rotor turns ratios (G_r=*68.1*).

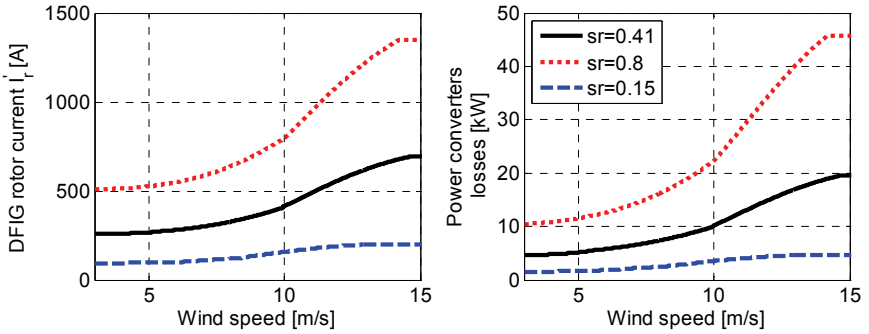

Fig. 21. DFIG rotor current and total power converters losses (RSC+GSC) versus wind speed, for three different stator to rotor turns ratios.

From simple analytical relations, neglecting stator and rotor losses and mechanical losses, it is possible to derive the well known rotor active power balance:

$$P_r = P_t \frac{s}{1-s} \tag{22}$$

With P_r the DFIG rotor active power. Since for the stator to rotor turns ratio analysis the gearbox ratio is maintained fixed, the super-synchronous maximal slip is the same between

solution with *sr=0.41* and *sr=0.8*, as it can be understood from Fig. 20 (d) (same maximal rotating speed). Therefore, referring to eq. (22), the rotor active power flow P_r is the same for both solutions on a wide operating wind speed (a difference can be noticed in the wind speeds region below 6 m/s as shown in Fig. 20 (d)). Neglecting the reactive power, the active power is the product of the rotor voltage and rotor current. However in one case (Gr=0.41) the rotor voltage is higher than in the other case (Gr=0.8), leading to a remarkable difference between the rotor currents behaviors, as presented in Fig. 21. This difference in currents produces a difference in the power converter losses which are strongly dependent on the currents. Therefore the global efficiency of the system decreased when sr is increased, explaining the annual production degradation illustrated in Fig. 19 for *sr* values above *sr=0.41*. Furthermore the increase in the RSC currents with the increase of *sr*, explains the increase of the power converter ratings presented in Fig. 19.
The gearbox mass issue was not considered here because its value is constant in the range of ratios used in these examples (according to the model presented in (4) and (5)). However the model can be very useful when the designers are exploring new topologies considering a wide range of gearbox ratios and stages (Aguglia et al., 2009). The objective of the analysis presented in this section was mainly to give a flavor of the complex selection process of some key variables of wind turbines DFIG drive systems. This complex process can be handled by use of a non-linear constrained optimization program, which can be used to select the optimal compromises between DFIG, power converter and gearbox performance/cost to maximize the annual production. The dimensional design of the DFIG itself, which consists in finding the optimal mechanical dimensions of the active materials (iron & copper), can be easily integrated in this global environment as presented by the authors in (Aguglia et al., 2009).

6. Conclusion

The DFIG drive components selection process, or design process, needs a global approach of the system in order to optimize its global performances. In the case of a wind turbine plant, such global performances are represented by the annual production, the overall mass and the initial cost. For this purpose the designer needs a model of each sub-component.
In this chapter only a few key variable for the DFIG drive design were considered for a sensitivity analysis with respect to the annual production and size of the converter. It is demonstrated that every choice of drive components (gearbox, DFIG and power converter) has an influence on the annual energy production and power converter cost. This powerful design methodology can be used to design the DFIG mechanical geometry as well. With this approach it is possible to integrate into the design process the wind probability distribution. Therefore, the plant is not optimized for a given operating point only, but for the global operation spectrum. This methodology is very useful for every electrical drive design in the variable speed application area, where all operating points must be considered and weighted with a certain probability of operation (e.g. typical torque vs. time behavior of an electric vehicle or typical cyclic operation of a fan).
The selection, or design, process can be coupled with a non-linear optimization algorithm, which can help in the complex task of selecting the optimal variables. In such an iterative process it is essential to have efficient models which allow to quickly obtaining all global performances. Analytical formulations of these models are well adapted for this purpose.
The presented results for DFIG wind turbines drives have been obtained thank to the proposed analytical determination of the rotor power converter control laws. The most

important variable influencing the annual production are the gearbox ratio and the DFIG stator to rotor turns ratio. It is important to mention that this sensitivity to these two variables is strongly dependent on the rotor side converter voltage limit. Therefore it is of extreme importance to take into account this limitation during the design process.

7. References

Aguglia D., Viarouge P., Wamkeue R., Cros J. (2007a). Selection of Gearbox Ratio and Power Converters Ratings for Wind Turbines Equipped With Doubly-Fed Induction Generators, IEEE conference "Electrical Machines and Drives – IEMDC", Vol. 1, 3-5 May 2007, pp. 447-452.

Aguglia D., Wamkeue R., Viarouge P., Cros J. (2007b). Optimizing the Annual Energy Production of Doubly-Fed Induction Generator Based Wind Turbines, IEEE Conference "Electrical Power Conference–EPC", Montreal, 25-26 October 2007, pp. 248-255.

Aguglia D., Viarouge P., Wamkeue R., Cros J. (2008). Analytical determination of steady-state converter control laws for wind turbines equipped with doubly fed induction generators, IET. Journal on Renewable Power Generation, Vol. 2, no 1, March 2008, pp. 16 -25.

Aguglia D., Viarouge P., Wamkeue R., Cros J. (2009). Doubly-Fed Induction Generator Drive Optimal Design for Wind Turbines with Reduced Gearbox Stages Number, "European Wind Energy Conference (EWEC)", 16-19 March 2009, pp. 1-10.

Çadirici I., and Ermis M.: 'Double-output induction generator operating at sub synchronous and super synchronous speeds: steady-state performances optimization and wind-energy recovery', *IEE Proceedings-B*, Vol. 139, No. 5, 1992

Cotrell J.R., "A preliminary evaluation of a multiple-generator drivetrain configuration for wind turbines," in *Proc. 21st ASME Wind Energy Symp.*, 2002, pp. 345-352.

Flender "Planurex® 2, Planetary gear units", Brochure, [Online]. Available: http://www.flender.com/_upload/k256en.pdf

Generation Using Doubly Fed Wound Rotor Induction Machine – A comparison With Alternative Schemes," *IEEE Trans. Energy Convers.*, Vol. 17, No. 3, 2002.

Grauers A., "Efficiency of three wind energy generator systems," *IEEE Trans. Energy Convers.*, Vol. 11, No. 3, September 1996.

Heier S.: "Grid integration of Wind Energy Conversion Systems, *Second edition,*" John Whiley & Sons, Ltd, 2006, pp. 31-44.

Li H., Chen Z., Polinder H. : 'Optimization of multibrid permanent-magnet wind generator systems', *IEEE Trans. on energy conv.*, Vol. 24, No. 1, March 2009, pp 82-92.

Pena R., Clare J. C., Asher G. M. (1996). Doubly fed induction generator using back-to-back PWM converters and its application to variable-speed wind–energy generation, *IET Journal on Electric Power Applications*, pp. 231-241, Vol. 43, no. 3

Petersson A., 'Analysis, modeling and control of doubly-fed induction generators for wind turbines', *Ph.D. Thesis, Chalmers University of Technology*, Sweden 2005.

Smith S., Todd R., Barnes M., and Tavner P. J.: 'Improved Energy Conversion for Doubly-Fed Wind Generators', *IEEE IAS Conference*, Vol. 4, 2005 Nordex N80/2500kW wind turbine Brochure, Online, Available: http://www.nordex-online.com/en/nordex/downloads.html, accessed November 2007

Zinger D. S. and Mulijadi E.: "Annualized Wind Energy Improvement Using Variable Speeds," *IEEE Trans. Ind. Appl.*, Vol. 33, No. 6, 1997.

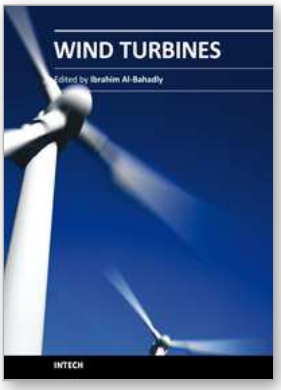

Wind Turbines

Edited by Dr. Ibrahim Al-Bahadly

ISBN 978-953-307-221-0
Hard cover, 652 pages
Publisher InTech
Published online 04, April, 2011
Published in print edition April, 2011

The area of wind energy is a rapidly evolving field and an intensive research and development has taken place in the last few years. Therefore, this book aims to provide an up-to-date comprehensive overview of the current status in the field to the research community. The research works presented in this book are divided into three main groups. The first group deals with the different types and design of the wind mills aiming for efficient, reliable and cost effective solutions. The second group deals with works tackling the use of different types of generators for wind energy. The third group is focusing on improvement in the area of control. Each chapter of the book offers detailed information on the related area of its research with the main objectives of the works carried out as well as providing a comprehensive list of references which should provide a rich platform of research to the field.

InTech Europe
University Campus STeP Ri
Slavka Krautzeka 83/A
51000 Rijeka, Croatia
Phone: +385 (51) 770 447
Fax: +385 (51) 686 166
www.intechopen.com

InTech China
Unit 405, Office Block, Hotel Equatorial Shanghai
No.65, Yan An Road (West), Shanghai, 200040, China
中国上海市延安西路65号上海国际贵都大饭店办公楼405单元
Phone: +86-21-62489820
Fax: +86-21-62489821